

One-dimensional localization of atoms in a standing spherical light wave

V. I. Balykin, Yu. E. Lozovik, Yu. B. Ovchinnikov, A. I. Sidorov, S. V. Shul'ga, and V. S. Letokhov

Institute of Spectroscopy, USSR Academy of Sciences, 142092 Troitsk, Moscow Region, USSR

Received April 17, 1989; accepted July 28, 1989

The localization of sodium atoms in a spherical standing single-frequency light wave was experimentally studied, and numerical calculations were performed for two- and three-level sodium atom models. A qualitative agreement was obtained between the experimental and theoretical results for the three-level atoms. The interaction between sodium atoms and the single-frequency field was shown to cause an effective localization of the atoms in the vicinity of the light-wave modes. The process was found to be influenced substantially by optical pumping, giving rise to an additional cooling of the atoms.

1. INTRODUCTION

Of the numerous schemes proposed for the localization of atoms and ions, the more attractive spectroscopically seem to be those whereby the motion of the particles is restricted to a region smaller than the radiation wavelength. With these atomic localization schemes, an interaction regime is achieved (the Lamb–Dicke regime) that allows the Doppler broadening of the atomic quantum transitions to be eliminated.

Such a localization scheme for atoms was proposed by Letokhov¹ and by Letokhov and Pavlik,² who suggested its use for the purpose of achieving a nonresonant standing light wave. Later, as the theory was developed further, the idea was extended to the case of quasi-resonant interaction between atoms and a standing light wave.^{3–5} At present the scheme is being studied extensively both experimentally^{6–8} and theoretically.^{4,9–12} Prentiss and Ezekiel⁶ detected an asymmetry in the fluorescence line shape of a beam of sodium atoms traversing a plane light wave at right angles. They explained this asymmetry as being due to the action on the atoms of the gradient force, causing the atomic concentration to rise in the vicinity of the nodes or loops of the wave. Salomon *et al.*⁷ used the absorption of an additional weakly resonant wave to determine the atomic density distribution in a standing light wave. The density of the atoms was found to increase near the nodes or loops of the standing wave, depending on whether the light frequency detuning was positive or negative with respect to the atomic transition frequency.

In Ref. 8 we demonstrated the one-dimensional localization of sodium atoms close to the nodes (or loops) of a standing spherical light wave and also their channeling along the nodes (or loops) of the curved wave front by observing the deviation of the atomic beam from its original propagation direction.

Here we present the results of a more detailed investigation into the localization of atoms in a quasi-resonant standing spherical light wave, along with the results of a numerical modeling of the localization process. In Section 2 we consider the basic idea and specific features of atomic localization in a plane and a spherical light wave and the conditions

necessary for its realization. Section 3 is devoted to the method of calculating atomic motion under our experimental conditions. A further description (Section 4) deals with the experimental setup and the techniques used to observe and measure the localization of the atoms. The results of a comparison between the experiment and the theoretical model are given in Section 5.

2. IDEA OF ATOMIC LOCALIZATION AND CONDITIONS NECESSARY FOR ITS REALIZATION

The motion of atoms in a standing light wave is governed mainly by the gradient (dipole) force, the friction force, and momentum diffusion.^{4,9,10,13} When the atomic transition saturation parameter is much less than unity and the field–atom interaction time is such that the change in the atomic momentum due to the friction force and diffusion is insignificant, both the friction force and momentum diffusion can be disregarded. In that case, an atom sees the light wave as a spatially periodic potential field, the period of which is equal to that of the spatial field intensity distribution, i.e., $\lambda/2$ [Fig. 1(a)]:

$$U(z) = U_0 \cos^2 kz, \quad (1)$$

where U_0 is the potential amplitude and $k = 2\pi/\lambda$. The motion of an atom in the potential field of a nonresonant standing light wave was treated by Letokhov¹ and, in more detail, by Letokhov and Pavlik.² An atomic ensemble placed in a potential field [Eq. (1)] is divided into two groups. The first group consists of atoms with a total energy of $W = E(z) + U(z) < U_0$, $E(z)$ being the kinetic energy of the atoms. These atoms reside between two adjacent maxima of the potential $U(z)$, the distance between which is $\lambda/2$, i.e., they are spatially localized. The localized atoms perform anharmonic oscillations with an amplitude less than $\lambda/4$ about the potential minima. The second group includes those atoms for which $W > U_0$. These atoms have an infinite motion, i.e., they are not localized. If the entire atomic ensemble has a continuous energy distribution, the localized and nonlocalized atoms are spatially intermixed.

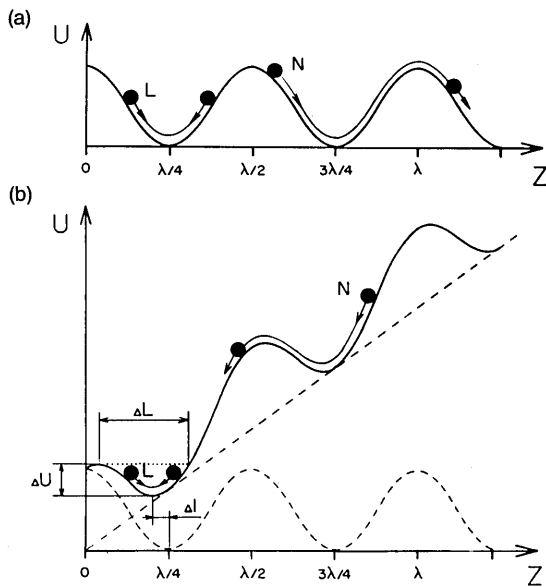


Fig. 1. Atomic localization in a standing light wave. (a) Localization in a plane wave. *L* denotes a localized atom oscillating near the bottom of a potential well, and *N*, a nonlocalized atom. (b) Localization in a spherical wave. The circular motion of the atoms gives rise to an effective centrifugal force, which causes the potential to change as shown by the solid curve. The force displaces the bottom of the potential well (Δl) and reduces its width (ΔL) and depth (ΔU).

Consider a standing wave placed in a uniform field wherein an atom is acted on by an additional force F along the z axis. This field may be a gravitational field, a homogeneous electric field (for ions), or, as in the present work (atomic motion in a spherical wave), the effective field of an inertial (centrifugal) force. In that case, the resultant potential field takes the form [Fig. 1(b)]

$$U(z) = U_0 \cos^2 kz + Fz. \quad (2)$$

The presence of the additional field has the following effects: First, it reduces the depth of individual potential wells [Fig. 1(b)] to

$$\Delta U = U_0 [1 - (F/U_0 k)^2]^{1/2} + (F/k) [\arcsin(F/U_0 k) - \pi/2], \quad (3)$$

where $U_0 k$ is the maximum gradient force in the standing wave in the absence of the external field. Second, it reduces the size of the potential wells to $\Delta L < \lambda/2$. Third, it shifts the position of the well bottom by an amount Δl [Fig. 1(b)]. When $F \ll U_0 k$, the shift of the position of the well bottom is given by the relation $\Delta l = F/M\omega_v^2$, where ω_v is the cyclic frequency of harmonic oscillations near the well bottom in the absence of the force F . Finally, what is most essential is the fact that the additional field gives rise to the force $\langle F \rangle$ averaged over the standing-wave period. This force accelerates the nonlocalized atoms and hence causes their eventual spatial separation from the localized atoms. This in turn makes it possible, first, to measure the atomic localization effect itself by observing the spatial separation of the atoms and, second, to isolate cold (localized) atoms from the entire atomic ensemble.

Let us now consider two-dimensional atomic motion in a standing wave formed by a laser beam with a Gaussian in-

tensity distribution (Fig. 2). It is not difficult to understand that in the case of a plane standing wave [Fig. 2(a)] the localization of atoms has practically no effect on such atomic beam parameters as divergence and shape.

Atomic localization in a spherical standing light wave occurs in a different manner [Fig. 2(b)]. Suppose that the atomic beam traverses the standing wave at a point far from the beam waist. Refer to the polar system of coordinates R, β [Fig. 2(b)]; the effective potential has the form of Eq. (2) with $z = R$. The force F in this case is the centrifugal force $F = Mv_t^2/R$, where M is the atomic mass and v_t is the tangential atomic velocity component. In the case of interest to us, this force can be considered to be constant because the radial motion of the atom in the standing wave takes place within a region approximately $\lambda \ll R$ across. All the conclusions drawn above about the motion of an atom in a plane standing light wave placed in a uniform field are therefore valid for the spherical standing wave. So the localization of atoms in a spherical standing light wave is possible when the gradient force exceeds the centrifugal force. Hence it follows that

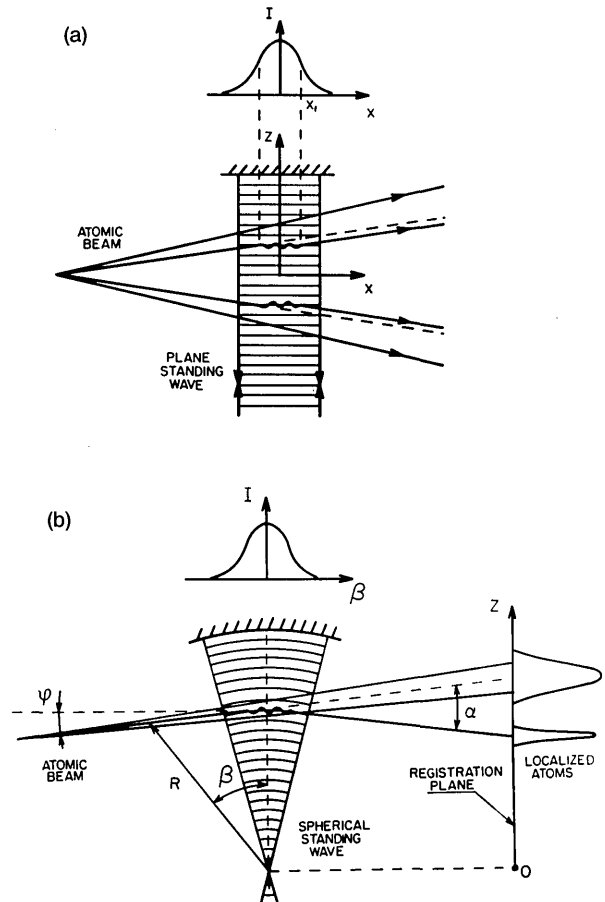


Fig. 2. (a) Localization of atoms in a plane standing light wave. (Top) Intensity distribution along the transverse coordinate of the laser beam forming the standing wave. x_1 is the distance from the laser beam center at which atomic localization occurs. (b) Localization of atoms in a spherical standing light wave. φ is the atoms' angle of entry into the standing wave, and α is the angle of deflection from the original atomic trajectory. In the course of localization, the atoms are divided into two ensembles, one containing cold, localized atoms and the other, hot, nonlocalized ones, followed by their spatial separation.

the longitudinal velocity of the atoms that can be localized is bounded above by the critical value

$$v_{cr} \simeq (F_g R/M)^{1/2}, \quad (4)$$

where F_g is the maximum gradient force in the standing wave.

The atoms entering the standing wave separate into localized and nonlocalized groups [Fig. 2(b)]. The nonlocalized atoms emerge from the wave in a direction close to the original propagation direction of the atomic beam, while their localized counterparts move along the nodes (or loops) of the wave, their original direction of motion being changed through an angle $\alpha \simeq 2\varphi$.

Thus an atomic beam interacting with a spherical standing light wave is split into two beams propagating at an angle φ to each other. It was this circumstance that we used to measure the effect of atomic localization in the wave. The maximum angle φ with which atomic localization is still possible is determined by the divergence of the standing wave:

$$\varphi_{max} \simeq w/R, \quad (5a)$$

where $2w$ is the diameter of the Gaussian beam forming the standing wave, measured at a distance R from the waist. The corresponding angle α is given by

$$\alpha_{max} = 2w/R. \quad (5b)$$

3. CALCULATION OF ATOMIC TRAJECTORIES IN THE STANDING WAVE

In our case, the motion of atoms in the standing wave can be calculated by using a quasi-classical approximation.¹⁰

In this approximation the problem is reduced to the integration of the Langevin equation

$$d\mathbf{p}/dt = \mathbf{F}, \quad (6)$$

where \mathbf{p} is the atomic momentum and \mathbf{F} is the total force acting on the atom, which may be represented in the form

$$\mathbf{F} = \mathbf{F}_g + \mathbf{F}_f + \mathbf{F}_d, \quad (7)$$

where \mathbf{F}_g is the gradient force, \mathbf{F}_f is that part of the total force that depends on the atomic velocity (i.e., friction force), and \mathbf{F}_d is the fluctuating force that is due to the atomic momentum diffusion.

A. Two-Level-Atom Approximation

The gradient force for a two-level atom is given by⁴

$$\mathbf{F}_g = \hbar\Omega[p/(1+p)]\alpha, \quad (8)$$

where $\Omega = \omega - \omega_0$ is the detuning of the light-wave frequency ω relative to the atomic transition frequency ω_0 ,

$$p = 2g^2/(\gamma^2 + \Omega^2) \quad (9)$$

is the local saturation parameter, $g = \gamma(2G)^{1/2}$ is the local Rabi frequency, $G = I/I_s$ is the ratio between the light-field intensity I and the saturation intensity I_s , 2γ is the natural atomic transition width, and

$$\alpha = \text{grad} \ln u, \quad (10)$$

where u is the local field amplitude in the standing wave.

The friction force for a two-level atom is expressed as

$$\begin{aligned} \mathbf{F}_f = & \hbar\Omega[p/(1+p)^3]\{2\gamma^2(1-p) - p^2(\Omega^2 + \gamma^2)\}/\gamma(\gamma^2 + \Omega^2)\} \\ & \times \{1/[1 + A(\Omega, p)(\alpha\mathbf{v}/\gamma)^2]\}(\mathbf{v}\alpha)\alpha = -\beta(\Omega, p, \alpha, \mathbf{v})(\mathbf{v}\mathbf{n})\mathbf{n}, \end{aligned} \quad (11)$$

where $\mathbf{n} = \alpha/|\alpha|$ and $\beta(\Omega, p, \alpha, \mathbf{v})$ is the friction coefficient. The expression for the friction force less the factor inside the second set of braces is the first term of the force expansion in terms of velocity,^{4,14} the factor allowing for higher orders of expansion. We also calculated this force by using the set of equations from Ref. 13. This allowed us to find the value of the coefficient $A(\Omega, p)$ to be approximately equal to 3 and to vary but little in our range of the parameters Ω and p . In our case the approximation is valid because the transverse velocity of the atoms is less than critical.^{5,15} The last term in Eq. (7) is the force due to the atomic momentum diffusion in both magnitude and direction, the fluctuation of the momentum during the time Δt being given by

$$\Delta\mathbf{p} = (2D_1 \Delta t)^{1/2}\xi_1\mathbf{n} + (2D_2 \Delta t)^{1/2}\xi_2\hat{u}, \quad (12)$$

where ξ_1 and ξ_2 are Gaussian-type random numbers, \hat{u} is a random unit vector,¹⁶

$$\begin{aligned} 2D_1 = & \hbar^2\alpha^2\gamma[p/(1+p)^3]\{1 + [4\gamma^2/(\gamma^2 + \Omega^2) - 1]p + 3p^2 \\ & + [(\gamma^2 + \Omega^2)/\gamma^2]p^3\}/[1 + A(\alpha\mathbf{v}/\gamma)^2] \end{aligned} \quad (13)$$

is the directional diffusion coefficient, and

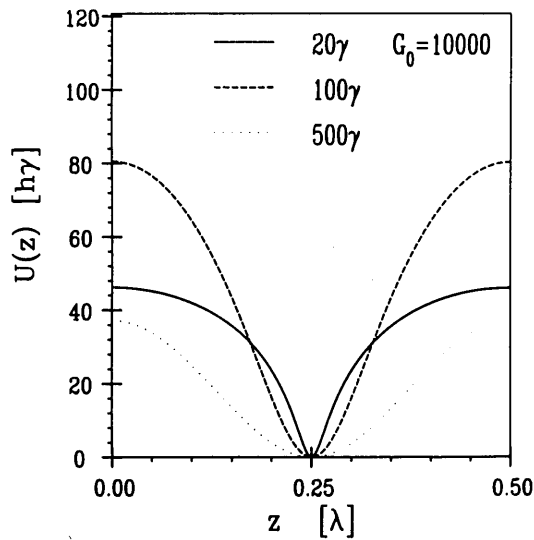
$$2D_2 = \hbar^2k^2\gamma[p/(1+p)]\{1/[1 + A(\alpha\mathbf{v}/\gamma)^2]\} \quad (14)$$

is the isotropic diffusion coefficient, with the atomic velocity dependence of the diffusion coefficient taken into account.

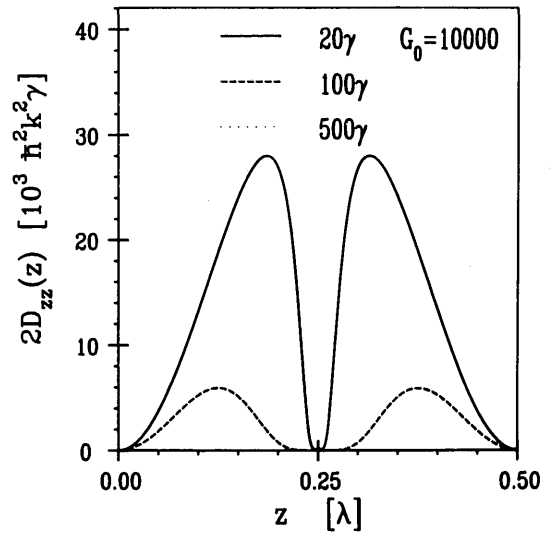
Figure 3 shows the spatial behavior of the standing-wave potential corresponding to the gradient force F_g [Fig. 3(a)], the friction coefficient [Fig. 3(b)], and the total diffusion coefficient for the saturation parameter in the traveling wave, G_0 , equal to 10^4 and for detunings of $\Omega = 20\gamma$, 100γ , 500γ [Fig. 3(c)]. It follows from a comparison of the curves that the deepest potential well is obtained with a detuning of $\Omega = 100\gamma$ [Fig. 3(a)]. It can be seen from Fig. 3(b) that the friction force is a damping force everywhere except in a small region near the standing-wave node, where the force is directed along the atomic velocity. The size of this region is determined by the relation $|p^2/(1-p)| < 2\gamma^2/(\gamma^2 + \Omega^2)$ [see Eq. (11)]. The friction force increases with the increasing detuning Ω , but so does the momentum diffusion [Fig. 3(c)].

Figure 4 illustrates the behavior of the potential energy of two atoms—localized (1) and nonlocalized (2)—in a standing spherical light wave, which reflects their trajectories in the laser field. The atoms spaced a distance $d = \lambda/2$ apart move parallel to each other and enter the field at points near the minima of two adjacent potential wells. The laser field parameters are as follows: laser power $P_L = 0.11$ W, frequency detuning $\Delta\nu = \Omega/2\pi = 400$ MHz, and radius of curvature of the wave front $R = 2$ m. The atoms differ in longitudinal velocity, the localized atom moving with a velocity $v = 500$ m/sec and its nonlocalized counterpart moving with a velocity $v = 1200$ m/sec. The increase of the longitudinal velocity of an atom enhances the centrifugal force acting on it in the coordinate system associated with the wave, which prevents the atom from being localized.

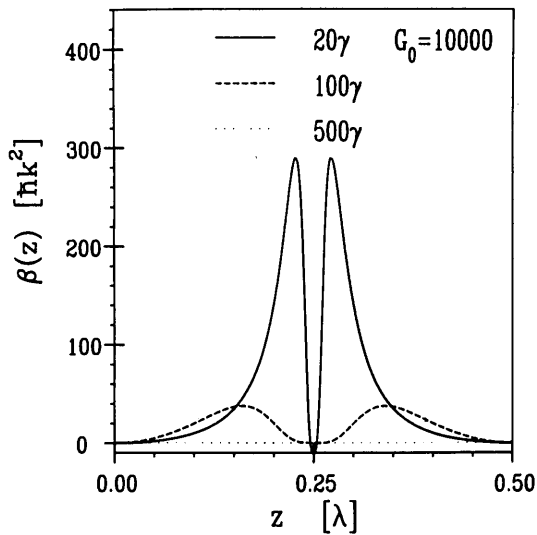
Figure 5 shows the change in transverse velocity under-



(a)



(c)



(b)

Fig. 3. Spatial behavior of (a) the atomic potential energy, (b) the friction coefficient, and (c) momentum diffusion in a standing light wave. G_0 is the atomic transition saturation parameter and $\Delta\nu$ is the positive frequency detuning. The curve for $\Delta\nu = 500$ MHz in (b) and (c) coincides with the x axis.

gone by localized [Fig. 5(a)] and nonlocalized [Fig. 5(b)] atoms on their entry into a spherical standing light wave, calculated by means of Eq. (6). The laser field parameters are as follows: $P_L = 0.11$ W, $\Delta\nu = 400$ MHz, $R = 4$ cm, and $v = 500$ m/sec. The atomic motion calculations were made both with and without taking the friction force into consideration.

The nonlocalized atom received a push in the region where the atomic trajectory is tangent to the wave front of the standing wave. The reason for this is that the atom is acted on by a gradient force of constant direction during a long period of time. The direction of this force determines the possibility of the atom's being localized or nonlocalized. Allowing for the friction force reduces the oscillation amplitude of the localized atom and substantially decreases the initial momentum increment of the nonlocalized one.

B. Three-Level Atom and Optical Pumping

All the formulas given above were derived for a two-level atomic model. In the case of a real, multilevel atom, there is another factor—optical pumping—that must be taken into

account. Our experiments were performed with sodium atoms undergoing the $3^2S_{1/2} \rightarrow 3^2P_{3/2}$ transition. A level diagram of this transition is presented in Fig. 6. The standing wave was produced by means of a linearly polarized laser field, the frequency of which was detuned by ~ 100 MHz to the blue side from the frequency of the $3^2S_{1/2}$ ($F = 2$) \rightarrow $3^2P_{3/2}$ ($F' = 3$) transition. This is the strongest transition, and the laser frequency detuning relative to the frequency of this transition is minimal compared with the rest of the transitions. For this reason we used in our calculations of the force acting on a sodium in the standing light wave a two-level atomic model with a transition frequency corresponding to the frequency of the actual $F = 2 \rightarrow F' = 3$ transition in the atom.

The standing light wave acted mechanically only on those atoms that were at the $F = 2$ sublevel in the ground state. If an atom moved to the $F = 1$ sublevel, it ceased interacting with the field and was lost to observation, because it was only the atoms in the $3^2S_{1/2}$ ($F = 2$) state that were detected in the experiment.

The probability of a transition to the $F = 1$ sublevel for

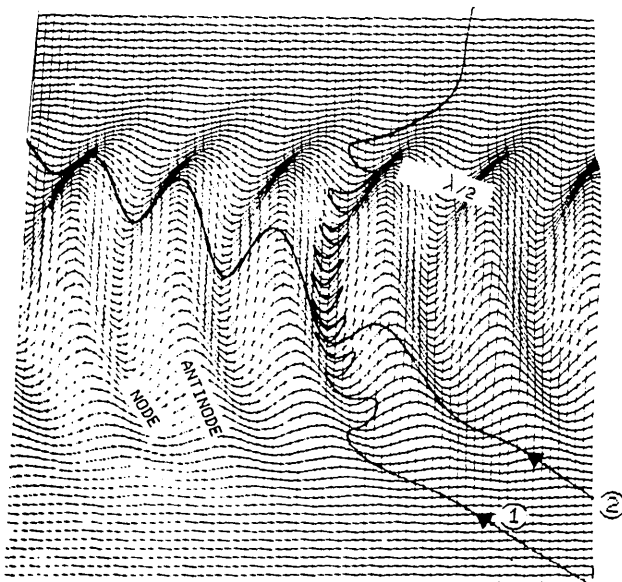


Fig. 4. Atomic potential energy in the spherical standing light-wave field for (1) a localized atom and (2) a nonlocalized one. Power in a single traveling wave, $P_L = 0.11$ W; $\Delta\nu = 400$ MHz; $R = 2$ m; laser beam diameter, $d = 1$ mm; localized atom velocity, $v_1 = 500$ m/sec; nonlocalized atom velocity, $v_2 = 1200$ m/sec. The curves reflect the trajectories of localized and nonlocalized atoms.

localized atoms differs substantially from that for their non-localized counterparts, the former moving mainly in the vicinity of the standing-wave nodes where the field intensity is materially lower than the wave-period-averaged intensity governing the optical pumping of the latter. It follows from consideration of the individual transition probabilities and selection rules that sodium atoms move to the $F = 1$ sublevel after being excited to the $3^2P_{3/2}$ ($F' = 2$) sublevel, followed by spontaneous relaxation to the $F = 1$ sublevel. Therefore, to take account of optical pumping, we used a three-level scheme whose transition frequencies corresponded to the actual $3^2S_{1/2}$ ($F = 2$) \rightarrow $3^2P_{3/2}$ ($F' = 2$) and $3^2S_{1/2}$ ($F = 1$) \rightarrow $3^2P_{3/2}$ ($F' = 2$) transitions. The theoretical relaxation rates γ_1 and γ_2 , corresponding to transitions from the $F' = 2$ sublevel to the sublevels $F = 1$ and $F = 2$, respectively, and the saturation intensity I_s , corresponding to the $F = 2 \rightarrow F' = 2$ transition, were selected by proceeding from the correspondence between the optical pumping measured experimentally for sodium atoms in the traveling wave and that calculated according to the three-level scheme. As a result, the following values were obtained: $\gamma_1 = 2 \times 4.25 \times 10^6$ sec $^{-1}$, $\gamma_2 = 2 \times 0.75 \times 10^6$ sec $^{-1}$ ($\gamma_1 + \gamma_2 = 3.14 \times 10^7$ sec $^{-1}$), and $I_s = 40$ mW/cm 2 .

We numerically calculated the localization of two- and three-level atoms in a one-dimensional spherical standing light wave. Figure 7 shows the atomic beam profiles produced after interaction with the spherical wave. The curves in the left-hand column refer to the two-level atoms, and those in the right-hand one to their three-level counterparts undergoing optical pumping. The atomic beam and laser field parameters were taken to be the same as in the experiment: the angular divergence of the atomic beam 3×10^{-3} rad, the angle of entry of the beam into the standing light wave $\varphi = 7.3 \times 10^{-3}$ rad, the laser field intensity $I = 20$ W/cm 2 , the radius of curvature of the light-wave front at the

point of intersection with the atomic beam $R = 40$ mm, and the laser beam diameter $2w = 0.6$ mm. The atomic beam profiles were calculated at a distance of $L_3 = 290$ mm from the atom-field interaction region and for three atomic velocity values: $v = 611, 800,$ and 1035 m/sec.

It can be seen from Fig. 7 that, after interacting with the standing light wave, the atomic beam gets split into two, so that the left-hand peak corresponds to localized atoms and the right-hand one to nonlocalized atoms. As the atomic velocity grows higher, the number of localized atoms decreases. One can comprehend this effect most simply by considering Fig. 1(b). The rise of the atomic velocity en-

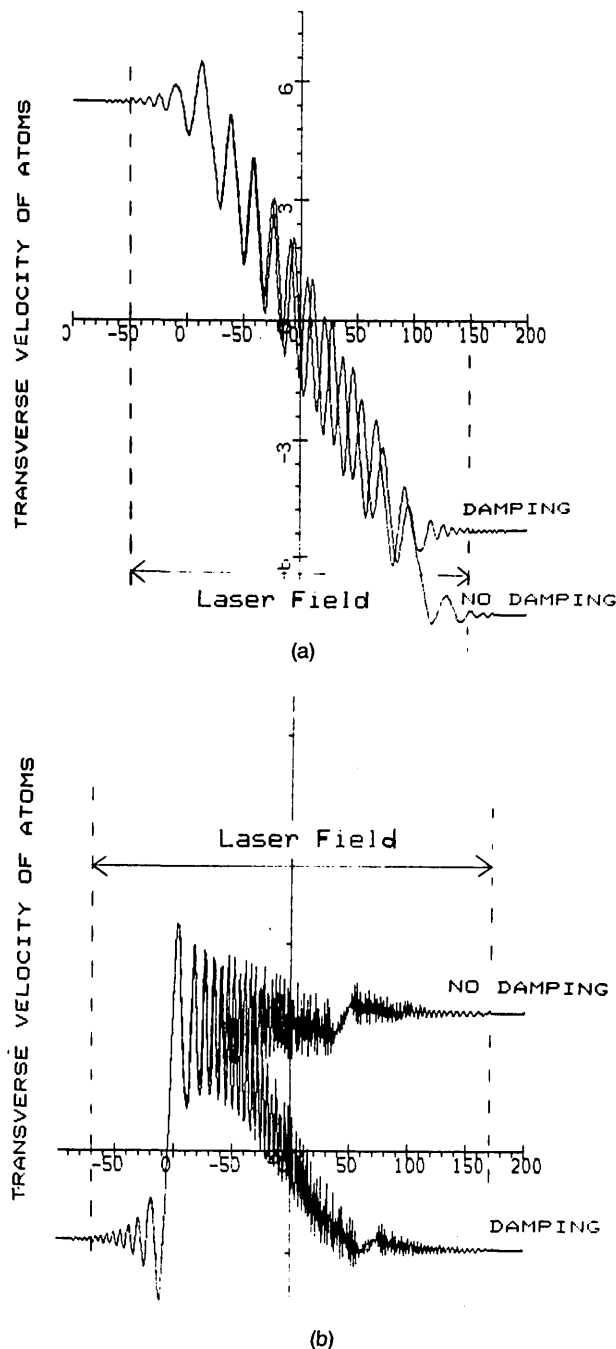


Fig. 5. Variation of the transverse velocity of (a) a localized atom and (b) a nonlocalized atom during their flight through the spherical standing light wave.

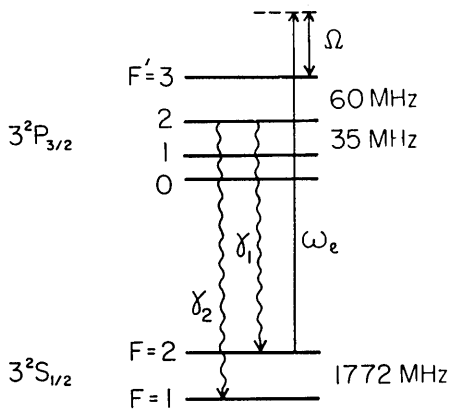


Fig. 6. Energy-level diagram of the ground and excited states of the sodium atom and position of the laser field frequency relative to the atomic transition frequency.

hances the centrifugal force acting on the atom, which in turn reduces the depth of potential wells in which atoms can be localized; see Eq. (3).

The absolute number of localized atoms depends on the effect of the atoms' being optically pumped from the sublevel $F = 2$ to the sublevels $F = 1$ (see Fig. 6) in the course of interaction with the standing light wave. The dashed curves in Fig. 7 show the atomic beam profiles in the absence of the standing-wave field (the peak amplitudes are reduced by a factor of 10). It can be seen that the optical pumping of the atoms, while having no effect on the character of atomic localization, changes the peak amplitudes for both localized and nonlocalized atoms. Comparison between the peak amplitudes for the localized two- and three-level atoms with velocities of 611 and 800 m/sec shows that the three-level atoms undergo no optical pumping, which means that they move in the vicinity of the standing-wave nodes where the field intensity is at a minimum.

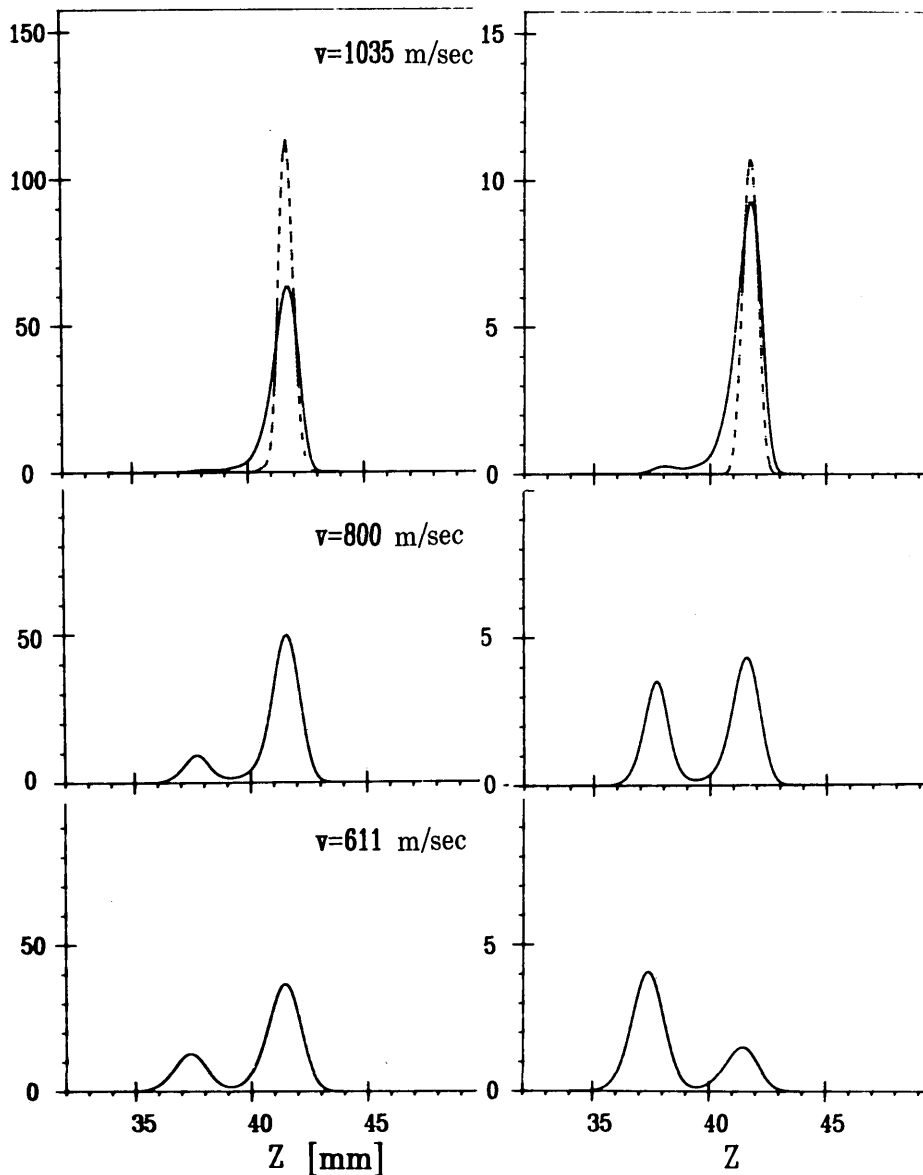


Fig. 7. Transverse atomic beam profile in the measured region as a function of the longitudinal atomic velocity. The column on the left contains beam profiles calculated for two-level atoms, and the one on the right, those calculated for three-level atoms with allowance made for optical pumping. The dashed curves correspond to no-laser-field conditions (the vertical scale is reduced by a factor of 10).

4. EXPERIMENTAL SETUP

The experimental setup is shown schematically in Fig. 8. To produce a spherical standing light wave, use was made of single-frequency radiation from a cw dye laser. The laser beam was focused with a lens ($F = 160$ mm) into the center of curvature of a spherical mirror ($R = 50$ mm). To eliminate parasitic feedback to the laser, the reflected laser beam was made to propagate at a small angle to the incident one in a plane normal to the atomic beam and then diaphragmed with a $200\text{-}\mu\text{m}$ slit placed in the focal plane of the lens. The standing-wave diameter (with reference to a factor-of- e^2 intensity reduction) at the site of intersection with the atomic beam was 0.6 mm, the wave-front radius of curvature being 40 mm.

The beam of sodium atoms was shaped by two diaphragms. The one in the atomic source was a round hole 4 mm in diameter. The other was a slit with dimensions $l_1 = 0.17$ mm and $l_2 = 0.5$ mm. The distance between the diaphragms was $L_1 = 290$ mm. In that case, the angular divergence of the atomic beam was 3×10^{-3} rad. The distance between the laser beam and the slit diaphragm was $L_2 = 10$ mm, the long side of the slit being parallel to the beam. The atomic source temperature was $T = 620$ K.

The atomic beam profile was measured by means of probe single-frequency radiation tuned to resonance with the $3^2S_{1/2} (F = 2) \rightarrow 3^2P_{3/2} (F = 3)$ transition. For this purpose, the probe beam focused with a long-focus lens was made to traverse the atomic beam at an angle of 76° and to scan it over an interval of 15 mm while remaining parallel to itself. The measured region was at a distance of $L_3 = 290$ mm from the standing light wave. The probe radiation frequency was set to fall within the Doppler absorption line contour of the atomic beam. In the experiment we measured the atomic fluorescence signal as a function of the coordinate of the point of intersection between the atomic and probe laser beams. The laser beam size (with reference to a factor-of- e^2 intensity reduction) was 0.2 mm.

Because the probe laser bandwidth was approximately 10 MHz, the probe beam resonated only with atoms moving with a certain longitudinal velocity, and so varying the probe laser frequency within the limits of the Doppler atomic absorption line contour made it possible to investigate the

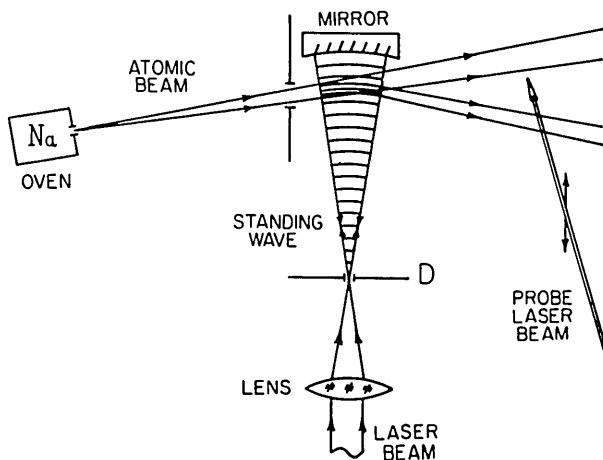


Fig. 8. Schematic of the experimental setup. D is the diaphragm used to eliminate feedback to the laser.

localization of atoms as a function of their longitudinal velocity.

The residual gas pressure in the vacuum chamber was some 10^{-6} Torr.

5. EXPERIMENTAL RESULTS AND THEIR COMPARISON WITH CALCULATION

Figure 9 presents the experimental results of the localization of sodium atoms in the spherical standing light wave. The curves are spatial profiles of the atomic beam in the measured region. The measurements were made for three atomic velocity values: $v = 611, 800,$ and 1035 m/sec. The laser intensity in the atom-field interaction region was 20 W/cm 2 .

It can be seen from the figure that, after interacting with the standing light wave, the atomic beam gets split into two, so that the left-hand peak corresponds to localized atoms and the right-hand one to nonlocalized atoms. This inference follows from comparison with the calculated curves (see Fig. 7) in which the left-hand peak represents the localized atoms and the right-hand one their nonlocalized counterparts. As can be seen, the distance between the peaks in experiment and theory agrees accurately enough. This distance is determined by the wave-front curvature and the size of the laser field in the atom-field interaction region. In our case ($R = 40$ mm, $2w = 0.6$ mm, $L_3 = 290$ mm), the distance between the peaks is [see relations (5)] $\Delta z = \alpha_{\max} L_3 = 4.3$ mm.

Comparison between the experimental curves and their theoretical counterparts calculated with due regard for the effect of optical pumping shows them to agree qualitatively well enough. At the same time, there are some differences. At an atomic velocity of 611 m/sec, the experimental peak corresponding to the localized is substantially narrower than its calculated counterpart. This difference is much smaller than what we found previously, 8 where no allowance was made in calculations for the velocity dependence of the atomic momentum diffusion coefficients. One possible explanation of the remaining discrepancy is a stronger effect of optical pumping on the atomic localization process.

Figure 10 shows the atomic beam profile in the measured region as a function of the atoms' angle of entry into the standing light wave, φ [see Fig. 1(b)]. The central profile corresponds to the optimum angle of entry, $\varphi_{\text{opt}} = 7.3 \times 10^{-3}$ rad, at which the number of localized atoms reaches its maximum. The dashed curves show the atomic beam profiles in the absence of the field forming the standing wave (the vertical scale is reduced by a factor of 10). The top and bottom profiles demonstrate that changing the angle of entry φ leads, first, to a decrease in the proportion of localized atoms and, second, to a change in the distance between the peaks due to localized and nonlocalized atoms.

As can be seen from Fig. 10, the position of the left-hand peak depends only slightly on the atoms' angle of entry into the wave. The reason is that in our case the divergence of the atomic beam is comparable with that of the standing wave. The variation of the distance between the peaks as a function of the angle agrees well with the simple estimate $\Delta z = 2(\varphi + \varphi_{\text{opt}})L_3$, where Δz is the distance between the peaks in the measured region located at a distance of L_3 from the standing light wave.

As can be seen from the top part of Fig. 10, there is a shift

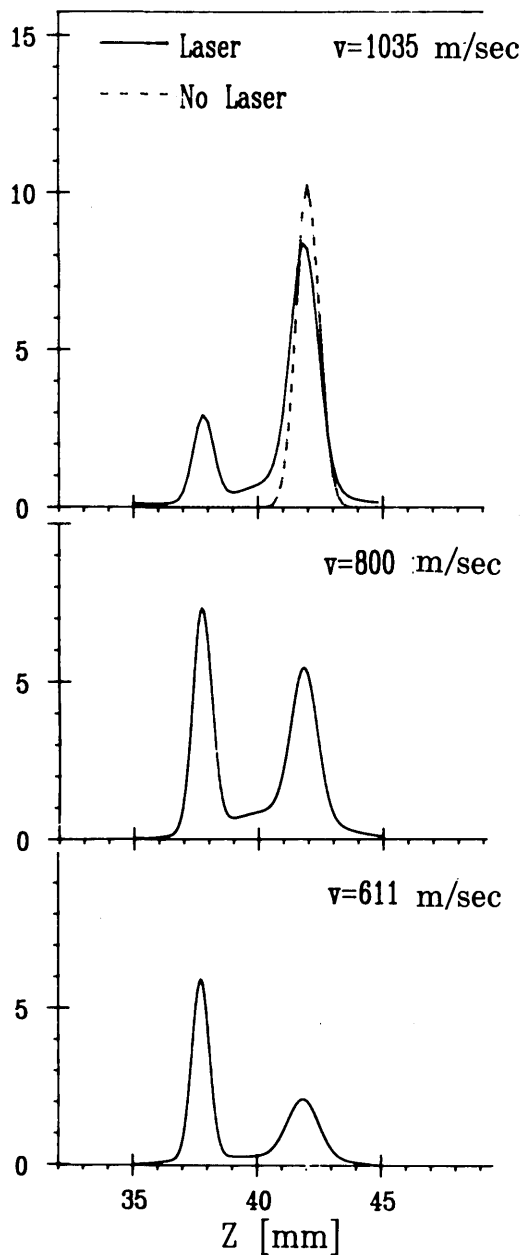


Fig. 9. Experimental atomic beam profiles in the measured region for various longitudinal atomic velocities. Laser frequency detuning, $\Delta\nu = 90$ MHz.

between the peak that is due to the nonlocalized atoms and the peak without the laser. An explanation for this phenomenon is shown in Fig. 5(b). When the angle of entry φ is small, the effect of the friction force is smaller than that of the push that the atom receives in the standing-wave potential. The calculation confirms this result.

We also studied the behavior of the localized atoms as a function of the laser field parameters. Figure 11 shows the atomic beam profile in the measured region as a function of the frequency detuning of the localizing laser field with respect to the atomic transition frequency. The columns on the left show experimental profiles, those in the middle contain profiles calculated with allowance made for optical pumping, and the right-hand columns show those calculated without regard to optical pumping. The measurements and

calculations were made for an atomic velocity of $v = 800$ m/sec and a laser field intensity of $I = 20$ W/cm². As follows from Eq. (8), variation of the laser field frequency changes the gradient force, causing the localization of atoms. In our experimental conditions the frequency detuning providing for the maximum potential is $\Delta\nu = 140$ MHz. As can be seen from the results of calculations made without consideration of optical pumping (right-hand column), it is exactly with this detuning that the number of localized atoms must be a maximum. And it is this situation that is observed in the experiment (see the curves for $\Delta\nu = 140, 240$ MHz). Moreover, the peak amplitudes for localized atoms are close to those calculated for no-optical-pumping conditions, which once more bears witness to the fact that the localized atoms move close to the bottom of potential wells. As the frequen-

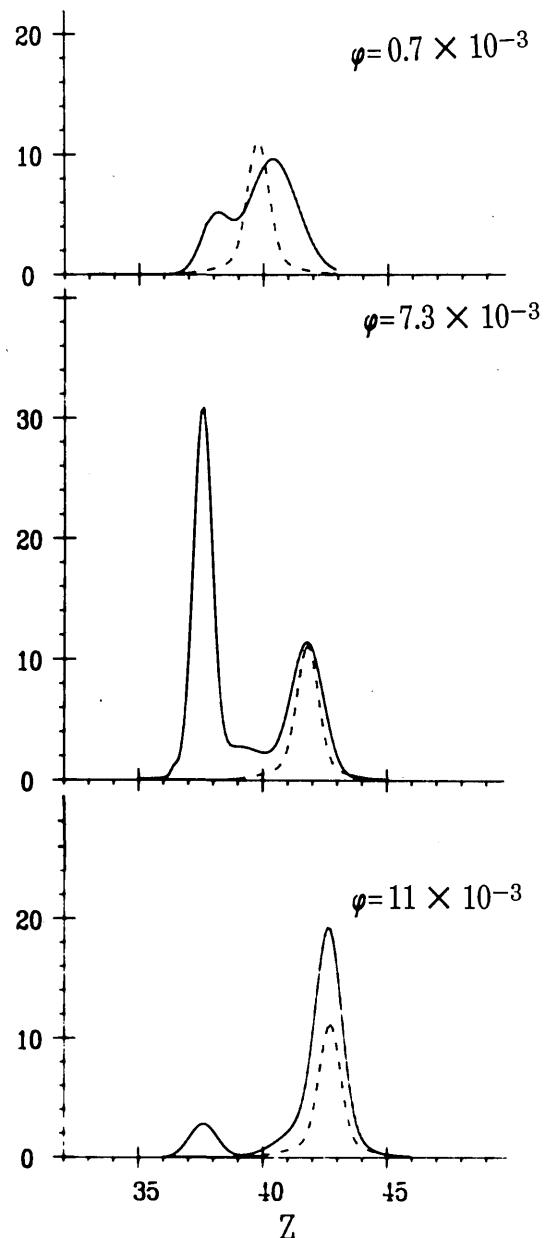


Fig. 10. Experimental atomic beam profiles for various angles of atomic beam entry into the standing light wave φ . Laser frequency detuning, $\Delta\nu = 140$ MHz.

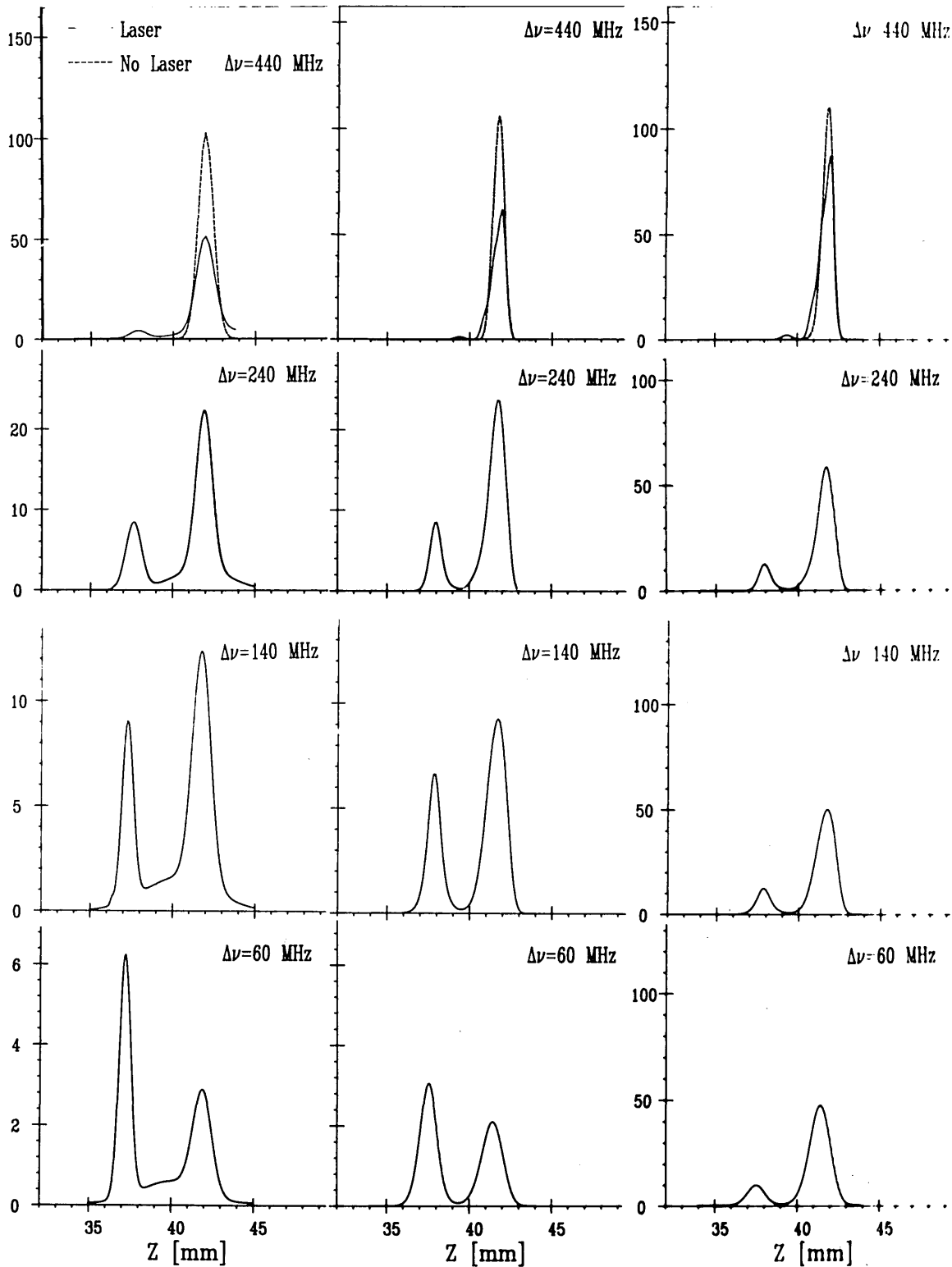


Fig. 11. Transverse atomic beam profile as a function of the laser field frequency detuning with respect to the atomic transition frequency. The column on the left shows experimental profiles, the one in the middle contains theoretical profiles calculated with consideration given to optical pumping, and the right-hand one shows calculated profiles for a two-level atom.

cy detuning is increased ($\Delta\nu = 440$ MHz) or reduced ($\Delta\nu = 60$ MHz) with respect to the optimal value, the number of localized atoms decreases in both theory and experiment. A satisfactory agreement is also observed between the experimental atomic profiles and their theoretical counterparts calculated with due regard for optical pumping (center column).

In the course of atom-field interaction, not only atomic localization but also the isolation of cold atoms occurs. One reason for this cooling is the fact that only those atoms can be localized in the standing wave whose transverse energy of is not greater than the potential barrier height. Another is the selectivity of the optical pumping process.

When experimenting with slower atoms one can observe the localization effect at lower laser field intensities. The minimum intensity at which the effect was still observable well enough was $I_{\min} = 1.3$ W/cm² at a frequency detuning of $\Delta\nu = 40$ MHz, the corresponding atomic velocity being $v_{\min} = 270$ m/sec. It was difficult to observe the effect at still lower laser field intensities in our experimental conditions, there being too few atoms moving with velocities below v_{\min} in the thermal atomic beam. The conditions of atomic localization under the minimum laser field intensity are sufficiently close to the molasses conditions,¹⁷ and therefore it appears that the effect of atomic localization in a three-dimensional standing light wave should also play a perceptible role.

6. CONCLUSIONS

We have presented the results of an investigation into the localization of sodium atoms in a spherical standing light wave. Based on a comparison between experimental and theoretically calculated atomic beam profiles, the atoms are convincingly demonstrated to undergo a sufficiently efficient localization and channeling along the light-wave front.

Studies of the effect of optical pumping on the localization process show that the localized atoms moving close to the bottom of potential wells are subject, unlike their nonlocalized counterparts, only to a weak pumping action.

ACKNOWLEDGMENT

The authors express their gratitude to S. Kittell for valuable assistance in preparing the manuscript.

REFERENCES

1. V. S. Letokhov, *Pis'ma Zh. Eksp. Teor. Fiz.* **7**, 348 (1968).
2. V. S. Letokhov and B. D. Pavlik, *Appl. Phys.* **9**, 229 (1976).
3. V. S. Letokhov and V. G. Minogin, *Appl. Phys.* **17**, 99 (1978).
4. J. P. Gordon and A. S. Ashkin, *Phys. Rev. A* **21**, 1606 (1980).
5. A. P. Kazantsev, V. S. Smirnov, G. I. Surdutovich, D. V. Chudennikov, and V. P. Yakovlev, *J. Opt. Soc. Am. B* **2**, 1731 (1985).
6. H. G. Prentiss and S. Ezekiel, *Phys. Rev. Lett.* **56**, 46 (1986).
7. C. Salomon, J. Dalibard, A. Aspect, H. Metcalf, and C. Tannoudji, *Phys. Rev. Lett.* **59**, 1969 (1987).
8. V. I. Balykin, V. S. Letokhov, Yu. B. Ovchinnikov, A. I. Sidorov, and S. V. Shui'ga, *Opt. Lett.* **13**, 958 (1988).
9. J. Dalibard and C. Cohen-Tannoudji, *J. Opt. Soc. Am. B* **2**, 1707 (1985).
10. V. G. Minogin and V. S. Letokhov, *Laser Light Pressure on Atoms* (Gordon & Breach, New York, 1987).
11. A. P. Kazantsev, G. I. Surdutovich, and V. P. Yakovlev, *Opt. Commun.* **68**, 103 (1988).
12. A. P. Kazantsev and I. V. Krasnov, *Pis'ma Zh. Eksp. Teor. Fiz.* **46**, 264 (1987).
13. V. G. Minogin and Yu. V. Rozhdestvensky, *Zh. Eksp. Teor. Fiz.* **93**, 1173 (1987).
14. A. P. Kazantsev, *Zh. Eksp. Teor. Fiz.* **66**, 1599 (1974).
15. J. Dalibard and C. Cohen-Tannoudji, *J. Opt. Soc. Am. B* **2**, 1707 (1985).
16. R. W. Hockney and J. W. Eastwood, *Computer Simulation Using Particles* (McGraw-Hill, New York, 1981).
17. S. Chu, L. Hollberg, A. Cable, and A. Ashkin, *Phys. Rev. Lett.* **55**, 48 (1985).